Frontiers in Bioscience Landmark

*Front. Biosci. (Landmark Ed)* **2026**; 31(1): 45680
https://doi.org/10.31083/FBL45680

*Original Research*

# *Akkermansia muciniphila* Ameliorates Chronic Sleep Deprivation-Induced Glucose Intolerance and Inflammatory Cytokine Activation

Zhenxing Wang[1,2], Yanhua Ma[1], Menglin Li[3], Xun Jiang[1,4], Qi Pan[1], Mingqun Deng[1,*], Lixin Guo[1,2,*]

[1]Department of Endocrinology, Beijing Hospital, National Center of Gerontology, Institute of Geriatric Medicine, Chinese Academy of Medical Sciences, 100730 Beijing, China
[2]Peking University Fifth School of Clinical Medicine, 100730 Beijing, China
[3]Department of Traditional Chinese Medicine, Beijing Hospital, National Center of Gerontology, Institute of Geriatric Medicine, Chinese Academy of Medical Science, 100730 Beijing, China
[4]Graduate School of Peking Union Medical College, Chinese Academy of Medical Sciences, 100191 Beijing, China
*Correspondence: mingqun_deng@163.com (Mingqun Deng); glxwork2016@163.com (Lixin Guo)
Academic Editor: Antoni Camins
Submitted: 10 August 2025 Revised: 26 December 2025 Accepted: 29 December 2025 Published: 21 January 2026

**Abstract**

**Objective**: Emerging evidence indicates that *Akkermansia muciniphila* (*A. muciniphila* or AKK) regulates host glucose metabolism through multiple pathways. In this study, we examined the therapeutic effects of *A. muciniphila* on chronic sleep deprivation (CSD)-induced glucose dysregulation and the underlying mechanisms. **Methods**: A modified multiplatform water environment method was used to generate a mouse model of CSD. The mice were divided into three groups: the control (CON) group (ad libitum sleep), the CSD group (subjected to sleep deprivation), and the CSD+AKK group (CSD mice were supplemented with *A. muciniphila* at $3 \times 10^8$ CFU per mouse, three times per week). After an 8-week intervention, glucose metabolism was assessed. Serum concentrations of lipopolysaccharide (LPS), interleukin-6 (IL-6), interleukin-1$\beta$ (IL-1$\beta$) and tumor necrosis factor $\alpha$ (TNF-$\alpha$) were measured. The mRNA expression and protein expression of mucin 2 (MUC2) and zonula occludens-1 (ZO-1) in the colon tissue were analyzed. Goblet cells in colon tissues were quantified using Alcian Blue–Periodic Acid-Schiff (AB–PAS) staining. Additionally, changes in gut microbiome diversity and composition among groups were compared. **Results**: CSD induced significant glucose intolerance and insulin resistance, evidenced by increased area under the curve (AUC) of the oral glucose tolerance test (OGTT), homeostatic model assessment of insulin resistance (HOMA-IR), and fasting insulin levels compared to the CON group (all $p < 0.05$). This was accompanied by a marked impairment of the colonic mucosal barrier, characterized by a profound loss of goblet cells and downregulation of key barrier components, MUC2 and ZO-1, at both the mRNA and protein levels (all $p < 0.05$). Intervention with *A. muciniphila* significantly ameliorated CSD-induced glucose intolerance, insulin resistance and colonic barrier damage. Furthermore, CSD elevated serum levels of LPS, IL-6, TNF-$\alpha$, and IL-1$\beta$ (all $p < 0.05$), which were effectively mitigated by *A. muciniphila intervention*. 16S rDNA sequencing confirmed the successful colonization of *A. muciniphila*, as its absolute abundance was significantly greater in the CSD+AKK group than in the CSD group. In addition, *A. muciniphila* intervention affected the abundance of *Burkholderiales bacterium*, *Lactococcus garvieae*, and other bacterial strains in the intestine. **Conclusion**: *A. muciniphila* supplementation effectively ameliorated CSD-induced glucose intolerance, reduced the serum levels of LPS and proinflammatory cytokines (IL-6, TNF-$\alpha$, and IL-1$\beta$), and restored intestinal barrier integrity by upregulating MUC2 and ZO-1 expression in colon tissues.

**Keywords:** glucose metabolism; sleep deprivation; *Akkermansia muciniphila*; inflammation; intestinal barrier functions

## 1. Introduction

A growing body of clinical and epidemiological evidence suggests that chronic sleep deprivation (CSD) is strongly associated with an increased risk of metabolic disorders such as insulin resistance and type 2 diabetes mellitus (T2DM) [1–3], posing potential challenges to public health [4,5]. While traditional research has focused on neurohormonal pathways [6–8], the precise mechanisms underlying CSD-induced glucose metabolic dysregulation remain incompletely elucidated, prompting exploration into novel pathological mediators.

Emerging insights point to gut microbiota dysbiosis as a critical intermediary in the metabolic disorder of sleep loss [9,10]. Sleep disorders may alter both the composition of the intestinal flora and its microenvironment, which in turn may disrupt host metabolic homeostasis [9,11,12]. Notably, studies have demonstrated that sleep deprivation compromises intestinal barrier integrity [13–15], which may lead to increased systemic translocation of endotoxins (e.g., lipopolysaccharide, LPS) and subsequent activation of inflammatory pathways [16–18]. These inflammatory responses are known to interfere with insulin

signaling, thereby promoting glucose intolerance [19,20]. This cascade highlights the gut microbiome as a promising therapeutic target for mitigating sleep deprivation-related metabolic complications.

Among the various gut symbionts, *Akkermansia muciniphila* (*A. muciniphila* or AKK) has garnered significant attention because of its potential beneficial effects on metabolic health [21]. *A. muciniphila* is an anaerobic bacterium renowned for its ability to fortify the intestinal mucosal barrier, exert anti-inflammatory effects, and regulate host glucose metabolism [22]. Clinical observations revealed a marked reduction in *A. muciniphila* abundance in individuals with prediabetes and diabetes compared with healthy controls [23]. Furthermore, multiple studies have indicated an association between decreased *A. muciniphila* levels and the occurrence of sleep disorders [24,25], suggesting its potential involvement in the sleep–metabolism axis. Mechanistically, *A. muciniphila* may enhance barrier function via extracellular vesicle secretion, reduce endotoxemia, and ameliorate insulin resistance [21,22,26]. These properties position *A. muciniphila* supplementation as a viable strategy to counteract metabolic disturbances.

In our prior investigation using a CSD mouse model (unpublished data), we observed a significant negative correlation between the abundance of *A. muciniphila* and glycemic parameters, indicating that it is a key modulator of CSD-induced glucose dysregulation. Building on this foundation and consistent with existing evidence on its barrier-preserving and metabolic-stabilizing functions, we hypothesize that *A. muciniphila* intervention could alleviate CSD-induced glucose intolerance and inflammatory activation. In this study, we therefore administered live *A. muciniphila* via oral gavage to CSD mice to evaluate its therapeutic effects on glucose metabolism and to preliminarily explore the underlying mechanisms, thereby addressing a critical knowledge gap in this evolving field.

## 2. Methods and Materials

### *2.1 Study Design and Experimental Protocol*

Thirty male C57BL/6J mice (6 weeks old, weighing 20 ± 1 g; C57BL/6J mice were supplied by the Laboratory Animal Center of Peking University Health Science Center) were randomly assigned to three groups (10 mice per group): the control (CON) group, CSD group, and CSD+AKK group (CSD mice with *A. muciniphila* oral gavage). The mice were housed under a 12:12-hour light–dark cycle (lights on from 7:00 to 19:00) and had free access to food and water.

We subjected the mice to CSD using a modified multiple-platform water environment method (**Supplementary Fig. 1**). CSD mice underwent 16 hours of daily sleep deprivation (17:00 to 9:00 the next day), with the remaining 8 hours (9:00–17:00) spent in standard cages for recovery, over an 8-week period [27,28]. CON group mice were housed in identical cages without sleep restriction. The CSD experiment began at 8 weeks of age (designated as week 0) and lasted for 8 weeks. At week 8, oral glucose tolerance tests (OGTTs) and insulin tolerance tests (ITTs) were performed. After the metabolic assessments were completed, blood was collected via the retro-orbital venous plexus under 3% isoflurane anesthesia, followed by euthanasia via cervical dislocation. For the CSD+AKK group, *A. muciniphila* suspension ($10^9$ CFU/mL) was administered via oral gavage (0.3 mL per time) three times per week during the CSD period. The CON and CSD groups received equal volumes of sterile phosphate-buffered saline (PBS, pH 7.2–7.4) as a control (Fig. 1A). All animal husbandry and experimental procedures were approved by the Institutional Animal Care and Use Committee of Peking University Health Science Center (Animal protocol approval number: DLASBE0510).

### *2.2 Assessment of Glucose Metabolism*

#### 2.2.1 OGTTs

After fasting overnight, the mice received an oral gavage of glucose solution (2 g/kg body weight). Blood glucose levels were measured from the tail vein immediately before (0 min) and at 15, 30, 60, 90, and 120 minutes after the administration.

#### 2.2.2 ITTs

The mice were placed in fresh bedding and fasted for 4 hours (water allowed), followed by intraperitoneal insulin injection (0.3 IU/kg body weight). Blood glucose was measured at 0, 15, 30, 60, 90, and 120 minutes using the same tail-tip blood sampling method (The detailed procedure for the emergency management of mouse hypoglycemia is described in Appendix A1).

#### 2.2.3 Homeostasis Model Assessment of Insulin Resistance (HOMA-IR) Index and Insulin Sensitivity (HOMA-IS) Index

Fasting serum insulin (INS) levels were quantified by enzyme-linked immunosorbent assay (ELISA); HOMA-IR was calculated as (FBG × INS)/22.5 and HOMA-IS was 22.5/(FBG × INS), with FBG representing fasting blood glucose concentration.

### *2.3 Reverse Transcription Quantitative Polymerase Chain Reaction (RT-qPCR)*

The tissue samples were homogenized in liquid nitrogen, followed by total RNA extraction using RNAiso Plus (9109; Takara Biomedical Technology, Beijing, China), chloroform phase separation, isopropanol precipitation, and 75% ethanol washing. cDNA was reverse transcribed under standardized conditions using the commercial kit (RR036A, Takara Biomedical Technology Co., Beijing, China). RT-qPCR analysis was performed with SYBR Green (RR820A, Takara Biomedical Technology Co., Bei-

jing, China) chemistry with prevalidated primers. GAPDH was used as the internal control and gene expression was quantified using the $\Delta\Delta$Ct method. The detailed reaction systems, thermal cycling parameters, and primer sequences are provided in **Supplementary Tables 1–4**.

### *2.4 Western Blot (WB) Analysis*

The tissue samples were homogenized in liquid nitrogen and subsequently lysed in RIPA buffer (AQ521; Aoqing Biotechnology, Beijing, China) with protease/phosphatase inhibitors (AQ551/AQ552; Aoqing Biotechnology, Beijing, China) for 30 minutes on ice. The protein concentration was quantified via a bicinchoninic acid assay (WB6501; NCM Biotech, Suzhou, China), as detailed in Appendix A2. The samples were subjected to sodium dodecyl sulfate–polyacrylamide gel electrophoresis after which the proteins were transferred to activated PVDF membranes (ISEQ00010; Merck Millipore, Darmstadt, Germany). The membranes were blocked in 5% skim milk, incubated with primary antibody (detailed antibody information is listed in Appendix A3) (4 °C overnight) and horseradish peroxidase (HRP)-conjugated secondary antibody (room temperature, 1 hour), and washed with TBST (137 Mm NaCl, 2.7 mM KCL, 25 mM Tris, 0.05% Tween-20) between steps (5 minutes $\times$ 5 times). The protein bands were quantified (densitometry measured by ImageJ 1.54k, National Institutes of Health, USA; https://imagej.nih.gov/ij/) and normalized relative to that of the housekeeping protein ($\beta$-tubulin) after enhanced chemiluminescence visualization (P10300; NCM Biotech, China).

### *2.5 Pathology Staining of Colon Tissue*

After the mice were sacrificed, the colon tissues were collected and fixed in 4% paraformaldehyde for 24 h, followed by paraffin embedding and sectioning.

#### 2.5.1 Hematoxylin and Eosin (H&E) Staining

Following dewaxing and rehydration, the paraffin sections were subjected to hematoxylin staining for 5 minutes, differentiated in 1% hydrochloric acid ethanol until they turned pink, and then blued in running water until the nuclei appeared clear and bright blue under microscopic examination. The sections were subsequently stained with eosin for 5 minutes, dehydrated through a graded series of ethanol solutions and xylene, and finally mounted with neutral gum. Colon tissues from different groups were observed under an optical microscope. A pathological evaluation was performed on H&E-stained colon sections according to a published scoring system [29], with the total histopathological score derived from the sum of the epithelium and infiltration scores.

#### 2.5.2 Immunohistochemistry (IHC) Staining

Paraffin-embedded sections were sequentially processed as follows: after dewaxing and rehydration, antigen retrieval was performed in citrate buffer (pH 6.0) using a microwave heating protocol (medium heat to boiling, maintained for 8 minutes, then medium–low heat for 7 minutes). After cooling, the sections were washed three times with PBS (pH 7.4). Endogenous peroxidase activity was then blocked by incubation in 3% hydrogen peroxide for 25 minutes at room temperature. Following a PBS wash, nonspecific binding was blocked with 3% bovine serum albumin for 30 minutes, prior to incubation with primary antibodies overnight at 4 °C. The sections were then incubated with an HRP-conjugated secondary antibody (ab205718/ab205719; Abcam, Cambridge, UK) for 50 minutes at room temperature, followed by diaminobenzidine development, hematoxylin counterstaining, dehydration, and mounting with neutral gum.

#### 2.5.3 Alcian Blue-Periodic Acid-Schiff (AB-PAS) Staining

Paraffin-embedded sections were dewaxed, rehydrated, and processed for AB–PAS staining. The procedure involved sequential staining with Alcian Blue (8 min), periodic acid (15 min), and Schiff's reagent (30 min in the dark), with a wash step after each staining step. After microscopic examination, the sections were dehydrated through an ethanol-butanol-xylene series and mounted in neutral gum. Quantitative analysis of goblet cells was carried out via ImageJ software.

### *2.6 ELISA*

We measured LPS, tumor necrosis factor-$\alpha$ (TNF-$\alpha$), interleukin-1$\beta$ (IL-1$\beta$), and interleukin-6 (IL-6) levels in mouse serum using a sandwich ELISA (CLOUD-CLONE CORP., Katy, TX, USA), while fasting serum insulin levels were quantified via a competitive inhibition assay, as described in Appendix A4.

### *2.7 In Vitro Cultures*

*A. muciniphila* (purchased from American Type Culture Collection, Catalog number: ATCC-BAA-835) was cultured anaerobically in CMC broth at 37 °C for 48 h (marked as P1). A 0.5 mL aliquot was transferred to fresh medium for P2 expansion. After 48 h, the bacterial cells were pelleted by centrifugation, resuspended in deoxygenated PBS, and adjusted to the target concentration ($1 \times 10^9$ CFU/mL, determined by the McFarland standard method).

### *2.8 16S rDNA Sequencing*

Absolute and relative quantification approaches for gut microbial 16S rDNA amplicon sequencing were integrated in this study. Absolute quantification was achieved by spiking synthetic DNA standards into samples during PCR amplification, enabling calibration curves to de-

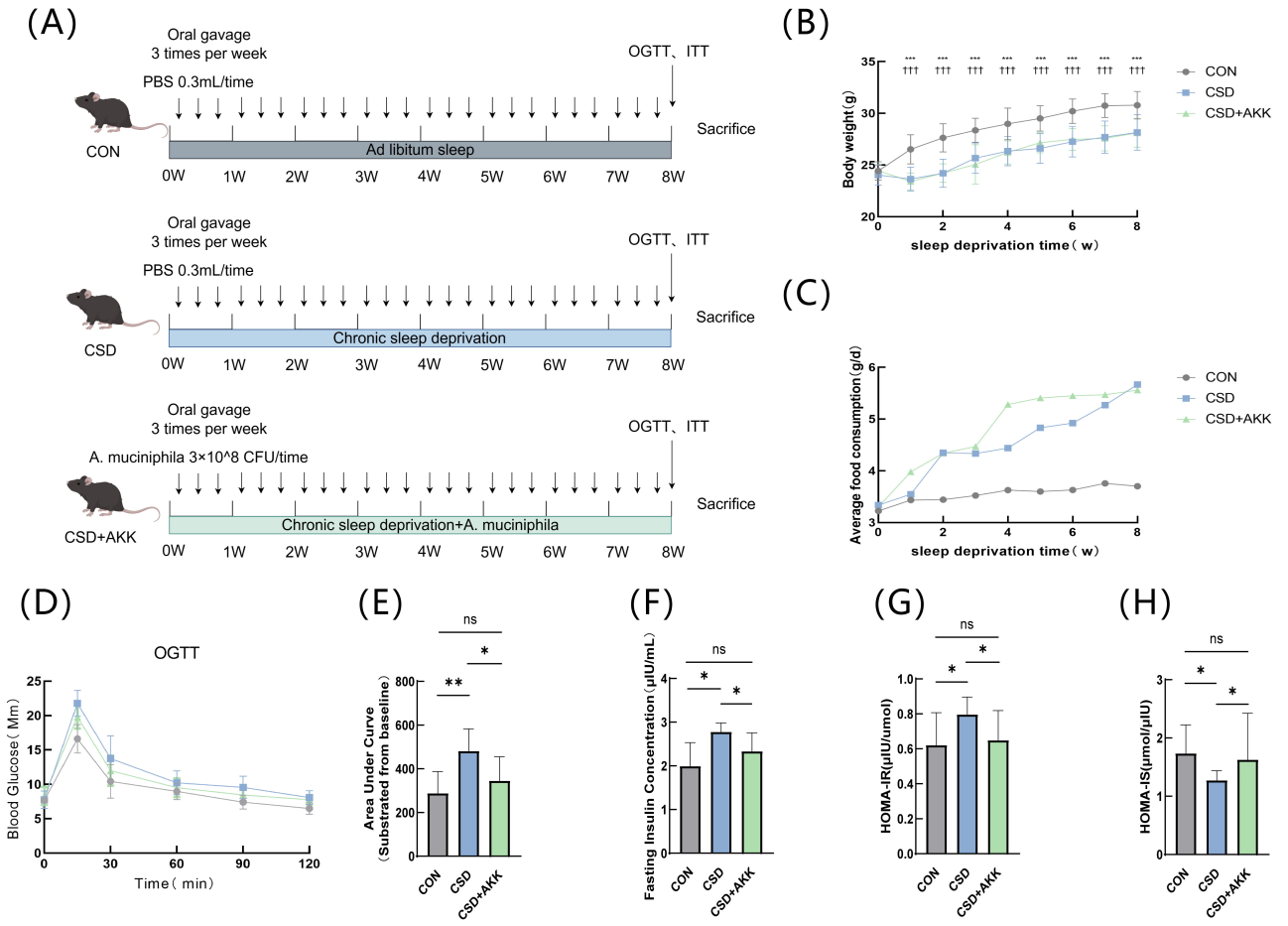


**Fig. 1. Effects of *A. muciniphila* on metabolic parameters *in vivo*.** (A) Overall experimental timeline. (B) Body weight changes (n = 10, mean ± SD). (C) Daily food consumption (n = 10, mean values). (D) Oral glucose tolerance test (OGTT) curves. (E) Area under the curve (AUC) value of the OGTT. (F) Fasting insulin concentration. (G) Homeostatic model assessment of insulin resistance (HOMA-IR). (H) Homeostatic model assessment of insulin sensitivity (HOMA-IS). Abbreviations: CON, control group; CSD, chronic sleep deprivation group; CSD+AKK, *A. muciniphila*-treated chronic sleep deprivation group. Statistical annotations: Panel (B): CSD vs. CON: *** $p < 0.001$; CSD+AKK vs. CON: ††† $p < 0.001$; Other panels: *$p < 0.05$, ** $p < 0.01$, ns, not significant (intergroup comparisons).

termine gene fragment copy numbers at both the DNA (copies/ng DNA) and sample levels (copies/g or mL). Relative quantification was performed following conventional amplicon sequencing workflows. Experimental procedures included genomic DNA extraction with quality control (gel electrophoresis validation), incorporation of spike-in standards for normalization, high-fidelity PCR library preparation with indexed primers, and Illumina sequencing. Bioinformatics analysis via QIIME2 involved adapter trimming (cutadapt), denoising, amplicon sequence variant (ASV)/operational taxonomic unit (OTU) generation, and taxonomic classification (rdp-classifier). Absolute abundance was calculated using spike-in-derived equations, followed by cellular abundance normalization (cell/g or mL). Community diversity was assessed through $\alpha$-diversity indices (Shannon, Chao1), $\beta$-diversity ordination (principal coordinate analysis, PCoA; nonmetric multidimensional scaling, NMDS), and statistical analyses (Wilcoxon; linear discriminant analysis effect size, LEfSe). Correlation analyses were explored using redundancy analysis (RDA), Mantel tests, and heatmaps, while compositional patterns were illustrated via phylogenetic trees, Venn diagrams, and stacked abundance plots.

### *2.9 Statistical Methods*

Continuous data are presented as the mean ± standard deviation (SD) or median (interquartile range, IQR). Comparisons between two groups were performed using Student's *t* test or Mann–Whitney *U* test. For multigroup comparisons, one-way analysis of variance (ANOVA) was applied, followed by post hoc pairwise tests (*Tukey's* test or *Dunnett's* test). A threshold of $p < 0.05$ was considered to indicate statistical significance. All the statistical analyses and graphing were conducted using SPSS 26 (IBM,

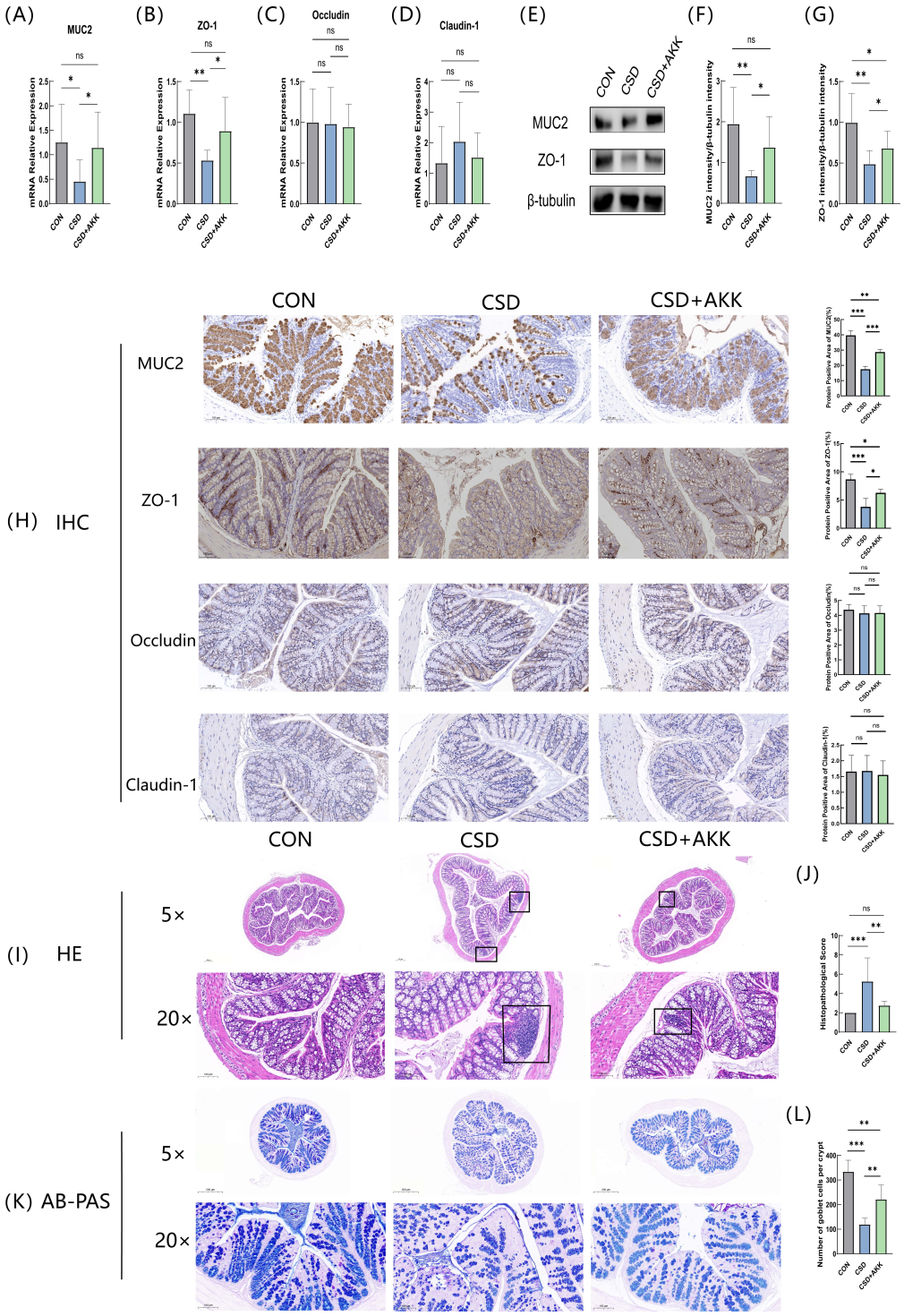


**Fig. 2. *A. muciniphila* restores colonic barrier integrity and ameliorates histopathological injury in CSD mice.** (A–D) Relative mRNA expression of (A) *MUC2*, (B) *TJP1* (encoding ZO-1), (C) *Ocln* (encoding Occludin), and (D) *Cldn1* (encoding Claudin-1) in colonic tissues. (E) Representative Western blot images of ZO-1 and MUC2 expression. (F,G) Quantification of (F) MUC2 and (G) ZO-1 protein levels normalized to those of $\beta$-tubulin. (H) Representative immunohistochemistry (IHC) staining images and quantitative analysis of MUC2, ZO-1, Occludin, and Claudin-1 expression. Scale bar, 100 µm. (I,J) Representative H&E staining images (black boxes indicate inflammatory cell infiltration) (I) and corresponding histopathological injury scores (J). Scale bars, 200 µm (5×) and 100 µm (20×). (K) Representative Alcian Blue-periodic acid–Schiff (AB–PAS) staining images. Scale bars, 500 µm (5×) and 100 µm (20×). (L) Quantification of goblet cell counts per crypt from AB–PAS-stained sections (20× magnification). All the data are presented as the mean ± SD (n = 10). $*p < 0.05$, $**p < 0.01$, $***p < 0.001$; ns, not significant. Group abbreviations: CON, control; CSD, chronic sleep deprivation; CSD+AKK, CSD with *A. muciniphila* intervention.

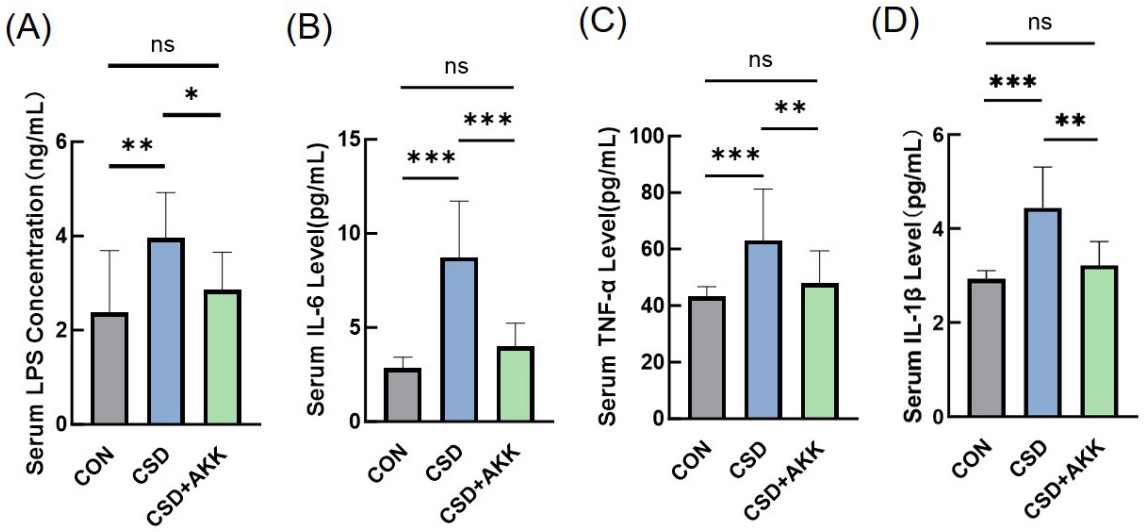


**Fig. 3. *A. muciniphila* attenuates CSD-induced systemic inflammation and endotoxemia.** Serum concentrations of (A) LPS, (B) IL-6, (C) TNF-$\alpha$, and (D) IL-1$\beta$. The data are presented as the mean $\pm$ SD (n = 10). *$p < 0.05$, **$p < 0.01$, ***$p < 0.001$; ns, not significant. Abbreviations: LPS, lipopolysaccharide; IL-6, interleukin-6; TNF-$\alpha$, tumor necrosis factor-alpha; IL-1$\beta$, interleukin-1 beta.

Chicago, IL, USA) and GraphPad Prism 8 (GraphPad Software, San Diego, CA, USA).

## 3. Results

### *3.1 A. muciniphila Ameliorates Glucose Intolerance and Insulin Resistance in CSD Mice*

Mice were subjected to 8-week CSD with concurrent *A. muciniphila* intervention to investigate subsequent changes in glucose metabolism (Fig. 1A). Compared with those in the CON group, a marked decrease in body weight ($p < 0.001$) and elevated daily food intake were observed in CSD-exposed mice. However, supplementation with *A. muciniphila* did not alter these parameters (Fig. 1B,C). Crucially, CSD-impaired glucose tolerance was demonstrated by higher blood glucose levels during an OGTT and a corresponding increase in the area under the curve (AUC) ($p < 0.01$). This metabolic disturbance was effectively mitigated by *A. muciniphila* intervention, which normalized both the glucose curve and the AUC value to those of the CON group (Fig. 1D,E). To further elucidate the mechanism underlying the increase in glucose tolerance, we measured fasting insulin levels and calculated the HOMA-IR and HOMA-IS indices. The CSD group exhibited hyperinsulinemia ($p < 0.05$) and significantly elevated HOMA-IR ($p < 0.05$), indicating a state of insulin resistance. *A. muciniphila* supplementation successfully counteracted these effects, significantly lowering fasting insulin ($p < 0.05$) and HOMA-IR ($p < 0.05$) levels and increasing HOMA-IS ($p < 0.05$), thereby restoring insulin sensitivity (Fig. 1F–H). However, the ITT assessment revealed no notable variation in insulin sensitivity among the groups (**Supplementary Fig. 2**).

### *3.2 A. muciniphila Restores CSD-Induced Colonic Mucosal Barrier Integrity*

Building upon the associations between metabolic health and gut barrier function, we assessed the key components of the colonic mucosal barrier. Our analyses revealed that CSD significantly impaired barrier integrity, an effect that was consistently reversed by *A. muciniphila* intervention. Specifically, CSD induced significant downregulation of the key barrier components MUC2 and ZO-1 at both the mRNA and protein levels (all $p < 0.01$; Fig. 2A,B,E–G). Notably, *A. muciniphila* intervention markedly attenuated these deficits by upregulating the expression of MUC2 and ZO-1. However, no significant changes in the mRNA expression of *Ocln* or *Cldn1* were detected among the three groups (Fig. 2C,D). Furthermore, the results of IHC also demonstrated a severe decrease in MUC2 and ZO-1-positive areas in the CSD group ($p < 0.001$), which was significantly mitigated by *A. muciniphila* treatment ($p < 0.001$ for MUC2; $p < 0.05$ for ZO-1; Fig. 2H).

This molecular-level disruption and recovery were further corroborated by tissue-level examinations. Histological assessment revealed significant CSD-induced inflammatory cell infiltration (assessed by histopathological score, CON vs. CSD $p < 0.001$) and a pronounced loss of goblet cells, which were markedly attenuated by *A. muciniphila* supplementation ($p < 0.01$; Fig. 2I–L).

### *3.3 A. muciniphila Mitigates Systemic Inflammation and Endotoxemia*

A compromised gut barrier often permits the translocation of microbial products, triggering systemic inflammation. We therefore measured serum markers of endotoxemia and inflammation. As hypothesized, the CSD group exhibited significant increases in the levels of circulating

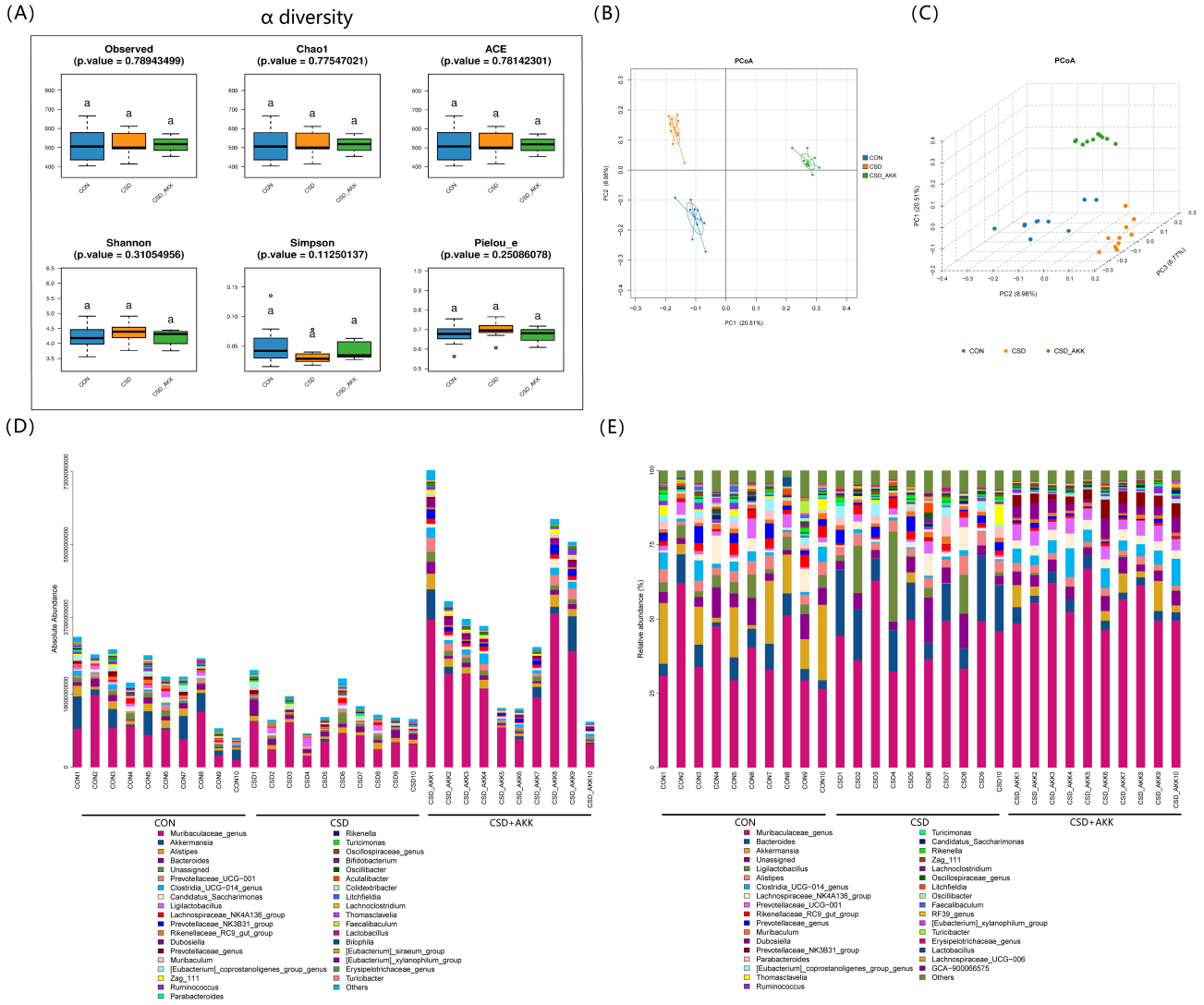


**Fig. 4. Effects of CSD and *A. muciniphila* intervention on gut microbiota composition.** (A) $\alpha$-Diversity indices (Chao1, ACE, Shannon, Simpson). The same lowercase letter "a" above the boxes indicates no statistically significant difference between any two groups ($p > 0.05$). (B) PCoA plot in two dimensions. (C) PCoA plot in three dimensions. (D) Heatmap of bacterial absolute bacterial abundance at the genus level. (E) Bar plot of bacterial relative abundance at the genus level. Abbreviations: CON, control; CSD, chronic sleep deprivation; CSD+AKK, CSD with *A. muciniphila* intervention; PCoA, principal coordinate analysis. n = 10 per group.

LPS ($p < 0.01$) and the proinflammatory cytokines IL-6, TNF-$\alpha$, and IL-1$\beta$ (all $p < 0.001$). Notably, *A. muciniphila* intervention significantly attenuated this systemic inflammatory response, reducing the serum levels of LPS ($p < 0.05$), IL-6 ($p < 0.001$), TNF-$\alpha$ ($p < 0.01$), and IL-1$\beta$ ($p < 0.01$) to levels comparable to those in the CON group (Fig. 3A–D).

### *3.4 A. muciniphila Modulates the Gut Microbiota Composition and its Correlation With Systemic Inflammation*

Finally, we explored whether the protective effects of *A. muciniphila* were associated with broader changes in the gut microbial ecosystem. While alpha diversity indices remained unchanged across groups (Fig. 4A), PCoA revealed distinct microbial communities among the CON, CSD, and CSD+AKK groups (Fig. 4B,C), indicating a shift in microbial composition.

Absolute and relative abundance analyses revealed specific taxonomic differences (Fig. 4D,E). The CSD+AKK group was characterized by enrichments of *Dubosiella* and *Tyzzeralla* at the genus level and of *Adlercerutzia equolifaciens* and *Bacteroides vulgatus* at the species level (Fig. 5). Notably, the absolute abundance of *A. muciniphila* itself was greater in the CSD+AKK group than in the CSD group, confirming successful colonization. Furthermore, the abundance of *Lactococcus garvieae* was significantly decreased after *A. muciniphila* supplementation (Fig. 6A).

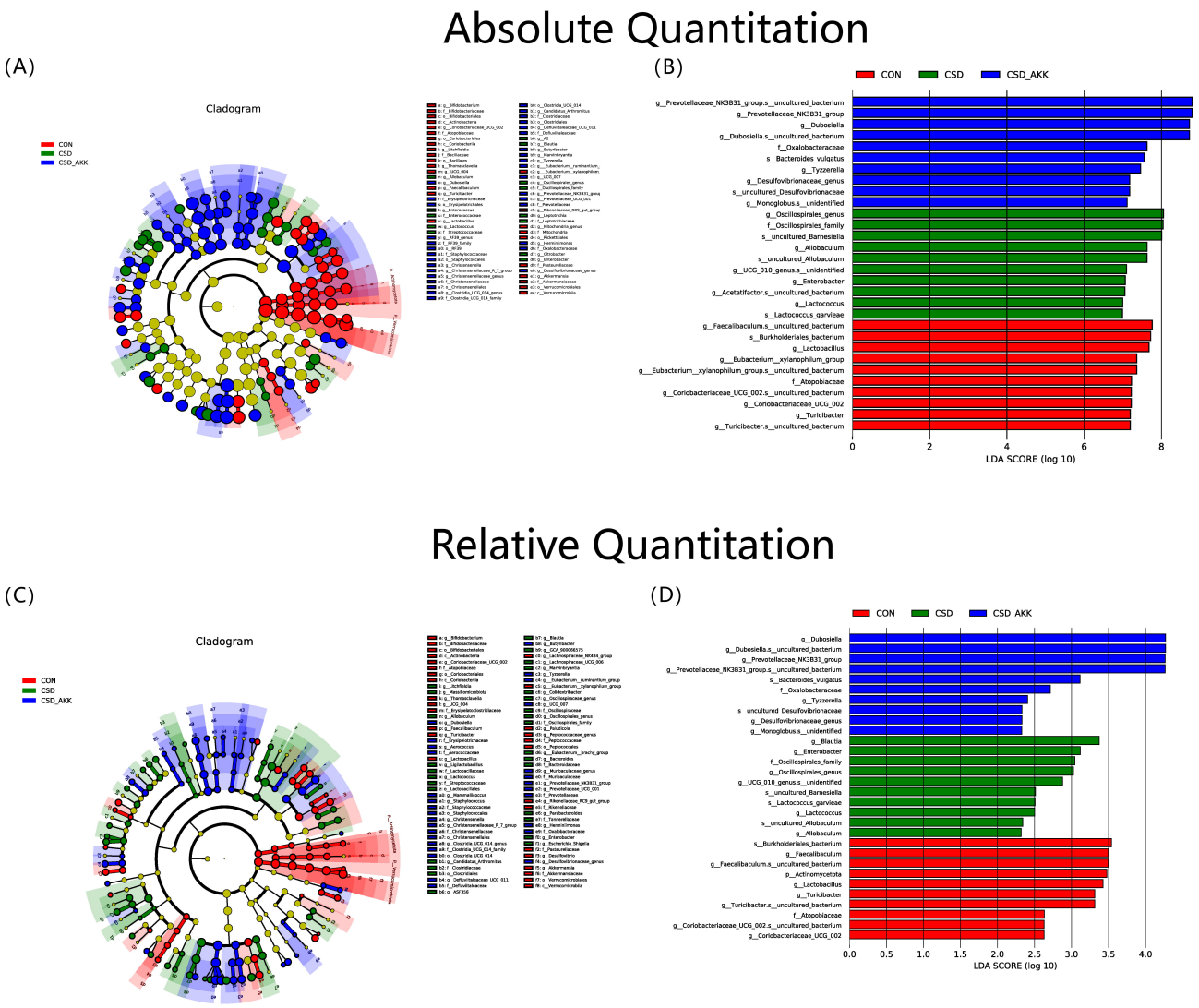


**Fig. 5. Differential microbial taxa identified by LEfSe analysis.** (A) Cladogram from LEfSe based on absolute abundance data. (B) Histogram of LDA scores from absolute abundance data. (C) Cladogram from LEfSe based on relative abundance data. (D) Histogram of the LDA scores from the relative abundance data. Abbreviations: CON, control; CSD, chronic sleep deprivation; CSD+AKK, CSD with *A. muciniphila* intervention; LDA, linear discriminant analysis; LEfSe, linear discriminant analysis effect size. n = 10 per group.

Most importantly, correlation analysis revealed a direct link between these microbial changes and the phenotype of CSD mice treated with *A. muciniphila*. The absolute abundance of *A. muciniphila* was strongly and negatively correlated with serum levels of LPS, IL-6, IL-1$\beta$, and TNF-$\alpha$. A similar beneficial correlation was observed for *Burkholderiales bacterium*, while *Lactococcus garvieae* was strongly positively correlated with the levels of all these inflammatory markers (Fig. 6B,C). These findings suggest that *A. muciniphila*-mediated amelioration of glucose intolerance and inflammation is closely associated with specific, beneficial remodeling of the gut microbiota.

## 4. Discussion

CSD has emerged as a pervasive environmental trigger for glucose metabolism disorders [30,31]. Consequently, identifying strategies to counteract CSD-induced metabolic abnormalities has become a focus of research. Given the established links between the gut microbiota, sleep, and glucose homeostasis, targeting the gut microbial ecosystem represents a promising therapeutic method. In this study, we demonstrate that supplementation with *A. muciniphila* effectively ameliorates CSD-induced glucose intolerance. The protective effects appear to involve intestinal barrier repair, with a consequent reduction in systemic inflammation.

On the basis of previous studies, *A. muciniphila* appears to be a bacterial strain particularly susceptible to environmental factors. Its abundance often decreases under various pathological conditions, including diabetes [32,33], hypertension [34], obesity [35], stress [36], anxiety [37], and sleep deprivation [24]. Consistent with prior find-

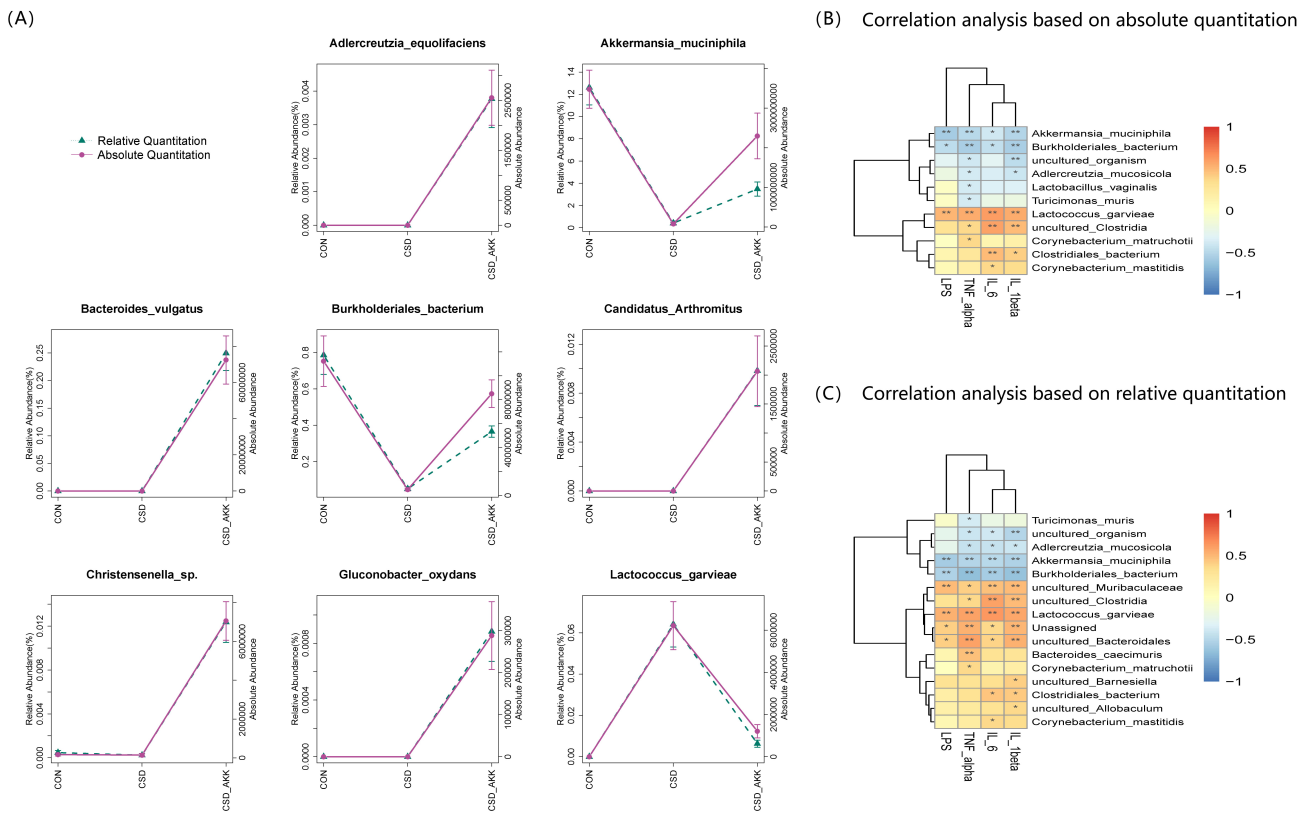


**Fig. 6. Species-level microbial alterations and their correlation with systemic inflammation.** (A) Differential bacterial species at the species level, showing only taxa whose abundance significantly changed according to both absolute and relative abundance analyses. (B) Correlation heatmap for the absolute abundance of differential species and serum levels of LPS and inflammatory cytokines. (C) Correlation heatmap for the relative abundance of differential species and serum levels of LPS and inflammatory cytokines. The data in (A) are presented as the mean ± SD (n = 10). The correlation strength in (B) and (C) is indicated by the color scale and Spearman's correlation coefficient. *$p < 0.05$, **$p < 0.01$.

ings [24,25,38,39], our data confirm that CSD significantly depletes this beneficial symbiont. From the perspective of the local microenvironment for bacterial colonization, intestinal epithelial inflammation and oxidative stress are likely significant factors influencing the abundance of *A. muciniphila* [12,24]. With respect to systemic factors, sleep deprivation could disrupt the rhythmic secretion of hypothalamic–pituitary–adrenal (HPA)–axis-related hormones [40,41] and melatonin [42–44], which may consequently impact the colonization of *A. muciniphila* [13,45]. Furthermore, relevant research has indicated that the abundance of *A. muciniphila* fluctuates with a certain circadian rhythmic fluctuation *in vivo* [46]. Sleep deprivation-induced disruption of circadian rhythms [47] and alterations in dietary patterns [46,48–50] could be other important factors influencing changes in *A. muciniphila* abundance.

Furthermore, a compromised intestinal mucosal barrier is likely a key mediator linking CSD to systemic inflammation activation and glucose intolerance. Multiple studies have indicated that CSD can lead to intestinal mucosal barrier damage [13,51,52]. Potential mechanisms underlying CSD-induced intestinal mucosal injury include inappropriate activation of intestinal inflammation [13,51], increased oxidative stress [52], and alterations in circadian rhythm regulators [53]. However, the aforementioned conclusions are primarily based on observational findings; they have not been mechanistically proven to establish causality, nor have they been validated in large-scale clinical studies. In a recent investigation, Zhang *et al.* [54] demonstrated by using a hypoxia-inducible factor 1-alpha (HIF-1$\alpha$) stabilizer in mice that HIF-1$\alpha$ inhibition might mediate sleep deprivation-induced intestinal mucosal barrier damage, further emphasizing the role of oxidative stress in this process. Notably, however, that Zhang *et al.* [54] utilized a 5-day sleep deprivation protocol, which differs somewhat from the CSD model used in our study. Therefore, whether these findings can be directly extrapolated to our experimental context requires further investigation.

A compromised intestinal barrier, a key consequence of CSD, facilitates the translocation of gut-derived endotoxins such as LPS into circulation [55]. Although we did not directly quantify LPS levels within the colonic tissue, the coincidence of structural barrier defects (loss of MUC2 and ZO-1) and functional systemic endotoxemia (elevated

serum LPS) strongly supports the "leaky gut" hypothesis in our model. This interpretation is consistent with the concept of "metabolic endotoxemia" established by Cani *et al.* [17], in which serum LPS is widely accepted as a surrogate marker for intestinal permeability and bacterial translocation. Consequently, the elevated proinflammatory cytokines observed in the serum likely originate from this gut-derived LPS triggering toll-like receptor 4 (TLR4) signaling, leading to the release of proinflammatory cytokines including TNF-$\alpha$ and IL-6 [17,56], and effectively linking the local barrier damage with the systemic metabolic phenotype. Our findings confirmed that *A. muciniphila* intervention robustly reduced serum LPS and inflammatory cytokine levels and concomitantly increased insulin sensitivity.

On the basis of existing research, *A. muciniphila* may modulate the host inflammatory factors through the following mechanisms: by degrading mucins while stimulating their production, thereby expanding the mucus layer [57]; by secreting extracellular vesicles that activate AMP-activated protein kinase (AMPK) in intestinal epithelial cells to increase tight junction protein expression [22]; and by producing anti-inflammatory metabolites that dampen immune activation [58]. The results presented here demonstrate the efficacy of *A. muciniphila* in restoring the expression of key barrier proteins, preventing goblet cell depletion in the colons, and mitigating systemic inflammation of CSD mice. Our study thus identifies *A. muciniphila* not only as a promising probiotic therapeutic but also as a key node in the complex pathophysiology linking sleep, the gut microbiota, and glucose metabolism.

Notably, we administered the intervention to mice via oral gavage of live *A. muciniphila*. Although this method has been widely used in previous studies and has been confirmed to effectively increase the colonization of *A. muciniphila* in the gut [58–60], how the bacteria survive the harsh gastric environment and successfully colonize the intestine remains incompletely understood. We speculate that repeated gavage and the dilution of gastric juice by the gavage vehicle (PBS, pH 7.2–7.4) may partially protect *A. muciniphila*, allowing a fraction of the bacteria to transit through the highly acidic stomach. On the other hand, it should be noted that the ameliorative effect of *A. muciniphila* on CSD-induced glucose metabolic abnormalities may not completely depend on successful colonization. *A. muciniphila*-derived proteins and extracellular vesicles [22,26] could also play a role in this process, although this study does not confirm whether these *A. muciniphila*-derived proteins or extracellular vesicles contributed to the observed effects.

As research on the metabolic regulatory mechanisms of *A. muciniphila* has advanced [61], its potential for clinical application has attracted increasing attention. A randomized controlled trial conducted by Depommier *et al.* [21] in overweight/obese volunteers demonstrated that *A. muciniphila* supplementation effectively improved insulin resistance and hyperinsulinemia and reduced total cholesterol and serum LPS levels. Another clinical study in overweight/obese individuals with T2DM revealed that the efficacy of *A. muciniphila* in reducing body weight and improving glucose metabolism was largely depended on the baseline abundance in the gut, with metabolic benefits observed only in those with low baseline *A. muciniphila* levels [62]. However, whether *A. muciniphila* confers metabolic benefits in humans under conditions of sleep disorder remains unclear, as no related clinical studies have been conducted. Some clinical reports suggest that probiotic supplementation may moderately improve sleep disturbances and related complications [63,64], however, the efficacy and safety of probiotic supplementation require further validation in large-scale trials. This study lays a preliminary groundwork for future research in this area.

This study has several limitations. First, the multiplatform water environment limits the use of metabolic cage systems for comprehensive energy expenditure measurements (e.g., $VO_2$ and $VCO_2$), thereby restricting our metabolic profiling to body weight and food intake. Second, although IL-6 is a known mediator of insulin resistance [65,66], our study did not investigate its downstream signaling pathways, such as the upregulation of suppressor of cytokine signaling 3 (SOCS-3), the phosphorylation status of insulin receptor $\beta$ (IR-$\beta$) and insulin receptor substrate-1 (IRS-1), or the activation of protein kinase B (PKB) and extracellular signal-regulated kinases 1 and 2 (ERK1/2) signaling [65,66]. Third, we acknowledge a significant limitation regarding the verification of local colonic inflammation. Owing to experimental constraints, we were unable to measure local inflammatory cytokine or LPS levels in the colonic tissue, nor did we perform *in vivo* permeability assays (e.g., FITC-dextran). We recognize that providing such local data would have strengthened the direct causal link between barrier injury and systemic inflammation. However, to address this gap, we integrated the histological evidence of goblet cells depletion and tight junction loss with the functional outcome of systemic endotoxemia. While this strongly implies a gut-origin mechanism, we caution that our conclusions regarding the "sequence" of pathological events are inferred from these combined systemic and structural markers, and future studies are warranted to directly validate the local inflammatory milieu. Fourth, while our findings support a beneficial role for *A. muciniphila,* the underlying mechanisms have not been fully elucidated, particularly concerning the involvement of microbial metabolites and host lipid metabolism. Finally, the exclusive use of a murine model and the absence of human samples represent a primary translational constraint.

This study provides a theoretical foundation for development of *A. muciniphila*-based interventions against CSD-induced metabolic dysregulation. Future investiga-

tions should aim to elucidate the precise underlying mechanisms of *A. muciniphila*, integrating multiomics approaches such as metagenomics, metabolomics (including short-chain fatty acids), and lipidomics to comprehensively explore its interactions with host metabolism. Furthermore, direct assessments of gut barrier function, oxidative stress, and detailed lipid metabolic profiles are warranted to elucidate the proposed pathways. Finally, clinical studies are essential to validate these findings in human populations and to explore the therapeutic potential of *A. muciniphila* for sleep-related metabolic disorders.

## 5. Conclusion

In conclusion, *A. muciniphila* intervention can effectively improve glucose intolerance induced by CSD. It can also significantly ameliorate the increase in serum endotoxin LPS and the increase in serum levels of the inflammatory factors IL-6, TNF-$\alpha$, and IL-1$\beta$ in CSD mice. Moreover, *A. muciniphila* intervention significantly abrogated the downregulation of the intestinal mucosal barrier proteins MUC2 and ZO-1 induced by CSD, partially alleviating damage to the intestinal mucosal barrier. Additionally, *A. muciniphila* intervention effectively increased the absolute abundance of certain bacterial strains, such as *Burkholderiales_bacterium* in the guts of CSD mice.

## Abbreviations

CSD, chronic sleep deprivation; CON, control; PBS, phosphate-buffered saline; OGTT, oral glucose tolerance test; HOMA-IR, homeostatic model Assessment of Insulin Resistance; HOMA-IS, homeostasis model assessment of insulin sensitivity; LPS, lipopolysaccharide; IL-6, interleukin 6; IL-1$\beta$, interleukin 1$\beta$; TNF-$\alpha$, tumor necrosis factor $\alpha$; ELISA, enzyme-linked immunosorbent assay; MUC2, mucin 2; ZO-1, Zonula Occludens-1; RT-qPCR, reverse transcription quantitative polymerase chain reaction; H&E, Hematoxylin and Eosin; WB, Western blot; IHC, immunohistochemistry; AB-PAS, Alcian Blue-Periodic Acid-Schiff; AUC, area under the curve; *A. muciniphila*, *Akkermansia muciniphila*; ITT, insulin tolerance test; SD, standard deviation; IQR, interquartile range; HPA, hypothalamic–pituitary–adrenal; HRP, horseradish peroxidase; ASV, amplicon sequence variant; OUT, operational taxonomic unit; ANOVA, one-way analysis of variance; PCoA, principal coordinate analysis; LDA, linear discriminant analysis; HIF-1$\alpha$, hypoxia-inducible factor 1-alpha; TLR-4, Toll-like receptor 4; AMPK, AMP-activated protein kinase; IRS, insulin receptor substrate; PKB, protein kinase B; ERK1/2, extracellular signal-regulated kinase 1/2; SOCS-3, suppressor of cytokine signaling 3.

## Availability of Data and Materials

The data used and analyzed during the current study are available from the corresponding author upon reasonable request.

## Author Contributions

ZXW was responsible for most of the experiments, study design, data analysis, visualization, and original draft writing. MQD was involved in the study design, analysis of microbiome data, original draft writing and funding acquisition. MLL was involved in the animal experiments, original draft writing and data analysis. YHM and XJ helped with the animal experiments and original draft writing. LXG and QP contributed to the study design, funding acquisition, and manuscript revision, and supervised the project. LXG was the lead contact of the study. All authors contributed to editorial changes in the manuscript. All authors read and approved the final manuscript. All authors have participated sufficiently in the work and agreed to be accountable for all aspects of the work.

## Ethics Approval and Consent to Participate

The animal protocol is in accordance with the current legislative regulations and is also in accordance with the NIH guidelines for the care and use of laboratory animals and was approved by the Institutional Animal Care and Use Committee of Peking University Health Science Center (animal protocol approval number: DLASBE0510).


## Acknowledgment

We thank Fei Xiao from the National Center of Gerontology (Beijing, China) for providing technical support for this study.

## Funding

This work was supported by the National High Level Hospital Clinical Research Funding (BJ-2022-145), the National Natural Science Foundation of China (82200928), and the China Endocrinology and Metabolism Young Scientific Talent Research Project (2021-N-03).


## Conflict of Interest

The authors declare no conflict of interest.

## Supplementary Material

Supplementary material associated with this article can be found, in the online version, at https://doi.org/10.31083/FBL45680.

## Appendix

See Appendices A1,A2,A3,A4.

**Appendix A1: Emergency Protocol for Hypoglycemia During the Mouse Insulin Tolerance Test (ITT)**

(1) Purpose

This protocol outlines the immediate and postprocedural actions required to manage unexpected hypoglycemia (blood glucose $\leq$3.0 mmol/L or ~54 mg/dL) and its severe

manifestations (e.g., lethargy, tremors, loss of righting reflex) during an ITT in mice. The primary goal is to ensure animal welfare and prevent mortality.

(2) Early Warning Signs of Hypoglycemia

Monitor the mice closely for the following signs, which may precede severe hypoglycemia:

- Tremors or shakiness
- Lethargy, inactivity, or slow movement
- Hunched posture
- Pallor (pale skin, especially on ears and paws)
- Ataxia (loss of coordination)

(3) Immediate Emergency Procedure

If a mouse exhibits severe hypoglycemia or any of the above signs, terminate the ITT immediately and take the following steps:

Step 1: Immediate Glucose Administration

- Procedure: Gently restrain the mouse and administer a single, intraperitoneal (IP) injection of 20% glucose solution at a dosage of 2 g of glucose per kg body weight.
- Rationale: Intraperitoneal injection ensures rapid absorption and is the most effective method for emergency rescue.

Step 2: Supportive Care and Monitoring

- Place the mouse on a warm pad or under a heating lamp (on a low setting) to prevent hypothermia. Ensure that it can move away from the heat source if needed.
- Do not return the mouse to its home cage until it is fully alert and mobile.
- Monitor the mouse continuously until it fully recovers (regains normal posture, mobility, and responsiveness). This may take 5–20 minutes.

Step 3: Confirm Recovery

- Once the mouse appears normal, a small drop of blood can be drawn to confirm that blood glucose has returned to a safe level (e.g., >4.0 mmol/L or ~72 mg/dL).
- Provide food on the cage floor for easy access.

Step 4: Postrecovery Observation

- House the mouse individually or with familiar cage mates for the next 24 hours.
- Continue to provide supplemental food and water on the cage floor.
- Monitor for any signs of relapse or abnormal behavior.

(4) Preventive Measures for Future ITTs

To prevent recurrence, consider the following adjustments for subsequent experiments:

- Re-evaluate Insulin Dose: The initial insulin dose (e.g., 0.75 U/kg for regular insulin) may be too high for your specific mouse model. A pilot test should be performed with a lower dose.
- Increase Sampling Frequency: Measure blood glucose levels more frequently (e.g., every 10–15 minutes) to catch a decreasing trend early.
- Set a Safe Termination Threshold: Pre-define a blood glucose concentration cutoff (e.g., 4 mmol/L or 72 mg/dL) at which the test will be stopped and glucose will be administered, *before* severe symptoms appear.
- Fasting Duration: Ensure the fasting period is standardized and not excessively long (typically 4–6 hours for mice).

(5) Documentation

- Record the incident in the animal's health record and the experimental log.
- Note the time of hypoglycemia onset, blood glucose level, dose and time of glucose administration, and the animal's recovery timeline.
- This documentation is crucial for animal welfare compliance and for refining your experimental protocol.

(6) Incidence (Hypoglycemia or Death) Rate: 0% (a total of 30 mice)

**Appendix A2: BCA Protein Quantification Assay**

(1) Bovine Serum Albumin (BSA) Standard Preparation:

The BSA stock solution was serially diluted using a dissolution medium identical in composition to that of the test samples (lysis buffer was used in this experiment) according to a predefined concentration gradient scheme, with concentrations set at 1, 0.5, 0.25, 0.125, 0.0625, 0.03125, and 0 mg/mL (marked as concentrations A–G).

(2) BCA Working Solution Preparation:

The required volume of color-developing reagent was calculated using the following formula: total reagent volume = (number of standards + number of test samples + 4) × number of replicates × 200 µL. Reagents A and B were mixed at a 50:1 volume ratio to prepare the working solution, which was thoroughly mixed before use.

(3) Quantitative Detection:

A total of 25 µL of each gradient BSA standard (concentrations A–G) and 2–10× diluted test samples were added to a 96-well plate. Afterward, 200 µL of working solution was dispensed into each well. The plate was sealed and incubated at 37 °C in the dark for 30 minutes. After the reaction system was allowed to equilibrate at room temperature for 5 minutes, the absorbance (OD value) was measured at 562 nm using a microplate reader. A standard curve was constructed on the basis of the relationship between the concentrations of the BSA standard and their corresponding OD values, and the protein concentrations of the test samples were subsequently calculated.

**Appendix A3. Reagents and Suppliers.**

| Reagents | Manufacturer | Catalog number | Dilution info |
|---|---|---|---|
| HRP-conjugated goat anti-rabbit/mouse IgG (H+L) | Abcam, Cambridge, UK | ab205718*/ab205719* | 1:50,000 (WB/IHC) |
| Zonula Occludens-1 (ZO-1) monoclonal antibody | Abcam, Cambridge, UK | ab276131* | IHC: 1:500<br>WB: 1:1000 |
| Occludin monoclonal antibody | Proteintech Group, Inc/Immunoway Biotechnology Co., Ltd. Suzhou, China | 66378-1-Ig (IHC)/YM8316 (WB) | IHC: 1:500<br>WB: 1:5000 |
| Claudin 1 monoclonal antibody | Proteintech Group, Inc/Immunoway Biotechnology Co., Ltd. Suzhou, China | 28674-1-AP (IHC)/YM8199 (WB) | IHC: 1:2000<br>WB: 1:1000 |
| Mucin2 (MUC2) monoclonal antibody | Abcam, Cambridge, UK | ab272692* | IHC: 1:2000<br>WB: 1:1000 |
| LPS ELISA kit | Biorigin (Beijing, China) Inc. | BN53434 | |
| TNF-$\alpha$/IL-1$\beta$/IL-6 ELISA kit | CLOUD-CLONE CORP., Katy, TX, USA | MEA133Mu/MEA563Mu/ MEA079Gu | |
| Insulin ELISA kit | CLOUD-CLONE CORP., Katy, TX, USA | CEA448Mu | |
| RNAiso Plus | Takara Bio Inc., Kusatsu, Shiga, Japan | 9109 | |
| TB Green Premix Ex Taq II (Tli RNaseH Plus) (2X Conc.) | Takara Bio Inc., Kusatsu, Shiga, Japan | RR820A | |
| 5X PrimeScript RT Master Mix | Takara Bio Inc., Kusatsu, Shiga, Japan | RR036A | |

*An asterisk (*) indicates that the antibody was used for both IHC and WB.

**Appendix A4: ELISA procedures**

After orbital blood was collected from the mice, the samples were centrifuged at 3500 rpm for 20 minutes at 4 °C. The supernatant was then collected, aliquoted, and stored. All serum samples were analyzed without dilution.

(1) Serum TNF-$\alpha$ Detection

The lyophilized standard was reconstituted with 0.5 mL of standard diluent and incubated at room temperature for 10 minutes to generate a 1000 pg/mL stock solution. A series of twofold serial dilutions were then prepared in EP tubes to obtain standard concentrations of 1000, 500, 250, 125, 62.5, 31.25, and 15.6 pg/mL, with the diluent serving as the blank control (0 pg/mL). Next, 100 µL of each standard, blank, or test sample was added to the microplate wells. The plate was covered and incubated at 37 °C for 60 minutes. After incubation, the liquid was discarded, and the plate was gently tapped dry. No washing was performed at this stage. Detection Solution A (biotinylated anti-TNF-$\alpha$ antibody) was diluted 1:100 to prepare Working Solution A. Then, 100 µL of Working Solution A was added to each well, followed by incubation at 37 °C for 60 minutes. After aspiration, each well was washed with 350 µL of Wash Buffer, and the buffer was left for 2 minutes before removal. This washing procedure was repeated three times. Similarly, Detection Solution B (HRP-conjugated avidin) was diluted 1:100 to obtain Working Solution B. A total of 100 µL of this solution was dispensed into each well, and the plate was incubated at 37 °C for 30 minutes. The liquid was then discarded, and the plate was washed five times as described above. For color development, 90 µL of TMB Substrate Solution was added to each well, and the plate was incubated at 37 °C in the dark for 10–20 minutes. The reaction was terminated by adding 50 µL of Stop Solution. The optical density at 450 nm was measured immediately using a microplate reader. The TNF-$\alpha$ concentrations in the samples were determined based on the standard curve derived from the OD values of the standards.

(2) Serum IL-6 Detection

The lyophilized standard was reconstituted in 1 mL of standard diluent and incubated for 10 minutes at room temperature to yield a 1000 pg/mL stock solution. A set of seven standard concentrations (500, 250, 125, 62.5, 31.25, 15.6, and 7.8 pg/mL) was prepared via serial dilution in EP tubes, using the diluent as a blank control (0 pg/mL). A volume of 100 µL of each diluted standard or test sample was added to the microplate wells. The plate was covered and incubated at 37 °C for 1 hour. After incubation, the liquid was discarded and the plate was gently tapped dry. No washing step was performed at this stage. Next, 100 µL of freshly prepared Working Solution A (biotinylated anti-IL-6 antibody) was added to each well. The plate was covered and incubated at 37 °C for 1 hour. Following incubation, the solution was aspirated, and each well was washed with 350 µL of Wash Buffer, which was left to soak for 2 min-

utes before removal. This washing procedure was repeated three times. Afterward, 100 µL of freshly prepared Working Solution B (HRP-conjugated avidin) was added to each well. The plate was covered and incubated at 37 °C for 30 minutes. After the solution was discarded, the plate was washed five times as described above. For color development, 90 µL of TMB Substrate Solution was added to each well, followed by incubation in the dark at 37 °C for 10–20 minutes. The reaction was stopped by adding 50 µL of Stop Solution per well. The optical density at 450 nm was measured immediately, and the IL-6 concentrations in the samples were calculated on the basis of the standard curve derived from the OD values of the standards.

(3) Serum LPS Detection

First, 50 µL of test samples, serially diluted standards, and blank controls (standard diluents) were added to the designated microplate wells. This was followed by the addition of 50 µL of HRP-conjugated antigen solution to each well. After sealing, the plate was incubated at 37 °C for 60 minutes. Following incubation, the liquid was discarded, and each well was washed with 300 µL of Wash Buffer, which was left to stand for 60 seconds before complete aspiration. The plate was then thoroughly tapped dry. This washing procedure was repeated for a total of five cycles. For color development, 90 µL of TMB Substrate Solution was added to each well, and the plate was incubated at 37 °C in the dark for 15 minutes. The reaction was terminated by the addition of 50 µL of Stop Solution per well, and the optical density at 450 nm was measured immediately using a microplate reader.

(4) Serum IL-1$\beta$ Measurement

The lyophilized standard was reconstituted with 1 mL of standard diluent and incubated at room temperature for 10 minutes to generate a 1000 pg/mL stock solution. A series of twofold serial dilutions were prepared in six EP tubes to obtain standard concentrations of 1000, 500, 250, 125, 62.5, 31.25, and 15.6 pg/mL, with the standard diluent serving as the blank control (0 pg/mL). Afterward, 25 µL of the standards, test samples, or diluent (blank) was added to the microplate wells. The plate was covered and incubated at 37 °C for 1 hour. After incubation, the liquid was discarded, and the plate was gently tapped dry without washing. Next, 25 µL of freshly prepared Working Solution A (biotinylated anti-IL-1$\beta$ antibody) was added to each well. The plate was covered and incubated at 37 °C for 1 hour. Afterward, the liquid was aspirated, and each well was washed with 100 µL of Wash Buffer, which was left to soak for 1–2 minutes before the plate was firmly tapped dry on absorbent paper. This washing procedure was repeated three times. Afterward, 25 µL of freshly prepared Working Solution B (HRP-conjugated avidin) was added to each well. After being covered and incubated at 37 °C for 30 minutes, the liquid was discarded, and the plate was washed five times as described above. Finally, 25 µL of TMB Substrate Solution was added to each well for color development. The plate was covered and incubated in the dark at 37 °C for 10–20 minutes. The reaction was stopped by the addition of 20 µL of Stop Solution per well, and the optical density at 450 nm was measured immediately.

(5) Insulin Measurement

The lyophilized standard was reconstituted with 0.5 mL of diluent and incubated at room temperature for 10 minutes to obtain an initial concentration of 500 pg/mL; a standard curve was then prepared via threefold serial dilutions to generate concentrations of 500, 166.67, 55.56, 18.52, and 6.17 pg/mL, using the diluent as the blank control (0 pg/mL). Subsequently, 50 µL of each standard or test sample was added to the microplate wells, followed by the addition of 50 µL of Working Solution A (biotinylated antigen solution), after which the plate was covered and incubated at 37 °C in the dark for 1 hour. Following incubation, the liquid was aspirated, and the wells were washed three times with 350 µL of Wash Buffer per well, which was allowed to stand for 1–2 minutes. After the wells were washed, 100 µL of working solution B (HRP-conjugated avidin) was added to each well and the plate was incubated at 37 °C for 30 minutes. The plate was then washed three more times, and 90 µL of TMB Substrate Solution was dispensed per well for color development in the dark at 37 °C for 10–20 minutes. The reaction was terminated by the addition of 50 µL of Stop Solution per well, and the optical density at 450 nm was measured immediately using a microplate reader. The insulin concentrations of the samples were ultimately determined on the basis of the standard curve fitted from the standard concentrations and their corresponding OD values.

## References


[1] Zuraikat FM, Laferrère B, Cheng B, Scaccia SE, Cui Z, Aggarwal B, *et al*. Chronic Insufficient Sleep in Women Impairs Insulin Sensitivity Independent of Adiposity Changes: Results of a Randomized Trial. Diabetes Care. 2024; 47: 117–125. https://doi.org/10.2337/dc23-1156.

[2] Kecklund G, Axelsson J. Health consequences of shift work and insufficient sleep. BMJ (Clinical Research Ed.). 2016; 355: i5210. https://doi.org/10.1136/bmj.i5210.

[3] Koren D, O'Sullivan KL, Mokhlesi B. Metabolic and Glycemic Sequelae of Sleep Disturbances in Children and Adults. Current Diabetes Reports. 2015; 15: 562. https://doi.org/10.1007/s11892-014-0562-5.

[4] Anauati MV, Gómez Seeber M, Campanario S, Sosa Escudero W, Golombek DA. The economic costs and consequences of (insufficient) sleep: a case study from Latin America. the European Journal of Health Economics. 2025; 26: 711–719. https://doi.org/10.1007/s10198-024-01733-8.

[5] Chalet F, Albanese E, Egea Santaolalla C, Ellis JG, Ferini-Strambi L, Heidbreder A, *et al*. Epidemiology and burden of chronic insomnia disorder in Europe: an analysis of the 2020 National Health and Wellness Survey. Journal of Medical Economics. 2024; 27: 1309–1320. https://doi.org/10.1080/13696998.2024.2407631.

[6] Hu Y, Lv Y, Long X, Yang G, Zhou J. Melatonin attenuates chronic sleep deprivation-induced cognitive deficits and HDAC3-Bmal1/clock interruption. CNS Neuroscience & Ther-

apeutics. 2024; 30: e14474. https://doi.org/10.1111/cns.14474.
[7] Ahmad AS, Ottallah H, Maciel CB, Strickland M, Doré S. Role of the L-PGDS-PGD2-DP1 receptor axis in sleep regulation and neurologic outcomes. Sleep. 2019; 42: zsz073. https://doi.org/10.1093/sleep/zsz073.
[8] Sang D, Lin K, Yang Y, Ran G, Li B, Chen C, *et al*. Prolonged sleep deprivation induces a cytokine-storm-like syndrome in mammals. Cell. 2023; 186: 5500–5516.e21. https://doi.org/10.1016/j.cell.2023.10.025.
[9] Zhao Y, Shu Y, Zhao N, Zhou Z, Jia X, Jian C, *et al*. Insulin resistance induced by long-term sleep deprivation in rhesus macaques can be attenuated by *Bifidobacterium*. American Journal of Physiology. Endocrinology and Metabolism. 2022; 322: E165–E172. https://doi.org/10.1152/ajpendo.00329.2021.
[10] Benedict C, Vogel H, Jonas W, Woting A, Blaut M, Schürmann A, *et al*. Gut microbiota and glucometabolic alterations in response to recurrent partial sleep deprivation in normal-weight young individuals. Molecular Metabolism. 2016; 5: 1175–1186. https://doi.org/10.1016/j.molmet.2016.10.003.
[11] Zhao D, Wang X, Liu H, Su M, Sun M, Zhang L, *et al*. Effect of circadian rhythm change on gut microbiota and the development of nonalcoholic fatty liver disease in mice. Sleep Medicine. 2024; 117: 131–138. https://doi.org/10.1016/j.sleep.2024.02.044.
[12] Wang X, Li Y, Wang X, Wang R, Hao Y, Ren F, *et al*. Faecalibacterium prausnitzii Supplementation Prevents Intestinal Barrier Injury and Gut Microflora Dysbiosis Induced by Sleep Deprivation. Nutrients. 2024; 16: 1100. https://doi.org/10.3390/nu16081100.
[13] Gao T, Wang Z, Dong Y, Cao J, Lin R, Wang X, *et al*. Role of melatonin in sleep deprivation-induced intestinal barrier dysfunction in mice. Journal of Pineal Research. 2019; 67: e12574. https://doi.org/10.1111/jpi.12574.
[14] Zhao N, Chen QG, Chen X, Liu XT, Geng F, Zhu MM, *et al*. Intestinal dysbiosis mediates cognitive impairment via the intestine and brain NLRP3 inflammasome activation in chronic sleep deprivation. Brain, Behavior, and Immunity. 2023; 108: 98–117. https://doi.org/10.1016/j.bbi.2022.11.013.
[15] Li L, Meng Z, Huang Y, Xu L, Chen Q, Qiao D, *et al*. Chronic Sleep Deprivation Causes Anxiety, Depression and Impaired Gut Barrier in Female Mice-Correlation Analysis from Fecal Microbiome and Metabolome. Biomedicines. 2024; 12: 2654. https://doi.org/10.3390/biomedicines12122654.
[16] Sun Q, Fan J, Zhao L, Qu Z, Dong Y, Wu Y, *et al*. *Weizmannia coagulans* BC99 Improve Cognitive Impairment Induced by Chronic Sleep Deprivation via Inhibiting the Brain and Intestine's *NLRP3* Inflammasome. Foods (Basel, Switzerland). 2025; 14: 989. https://doi.org/10.3390/foods14060989.
[17] Cani PD, Amar J, Iglesias MA, Poggi M, Knauf C, Bastelica D, *et al*. Metabolic endotoxemia initiates obesity and insulin resistance. Diabetes. 2007; 56: 1761–1772. https://doi.org/10.2337/db06-1491.
[18] Chen G, Ran X, Li B, Li Y, He D, Huang B, *et al*. Sodium Butyrate Inhibits Inflammation and Maintains Epithelium Barrier Integrity in a TNBS-induced Inflammatory Bowel Disease Mice Model. EBioMedicine. 2018; 30: 317–325. https://doi.org/10.1016/j.ebiom.2018.03.030.
[19] Hotamisligil GS, Peraldi P, Budavari A, Ellis R, White MF, Spiegelman BM. IRS-1-mediated inhibition of insulin receptor tyrosine kinase activity in TNF-alpha- and obesity-induced insulin resistance. Science (New York, N.Y.). 1996; 271: 665–668. https://doi.org/10.1126/science.271.5249.665.
[20] Jager J, Grémeaux T, Cormont M, Le Marchand-Brustel Y, Tanti JF. Interleukin-1beta-induced insulin resistance in adipocytes through down-regulation of insulin receptor substrate-1 expression. Endocrinology. 2007; 148: 241–251. https://doi.org/10.1210/en.2006-0692.
[21] Depommier C, Everard A, Druart C, Plovier H, Van Hul M, Vieira-Silva S, *et al*. Supplementation with Akkermansia muciniphila in overweight and obese human volunteers: a proof-of-concept exploratory study. Nature Medicine. 2019; 25: 1096–1103. https://doi.org/10.1038/s41591-019-0495-2.
[22] Chelakkot C, Choi Y, Kim DK, Park HT, Ghim J, Kwon Y, *et al*. Akkermansia muciniphila-derived extracellular vesicles influence gut permeability through the regulation of tight junctions. Experimental & Molecular Medicine. 2018; 50: e450. https://doi.org/10.1038/emm.2017.282.
[23] Corb Aron RA, Abid A, Vesa CM, Nechifor AC, Behl T, Ghitea TC, *et al*. Recognizing the Benefits of Pre-/Probiotics in Metabolic Syndrome and Type 2 Diabetes Mellitus Considering the Influence of *Akkermansia muciniphila* as a Key Gut Bacterium. Microorganisms. 2021; 9: 618. https://doi.org/10.3390/microorganisms9030618.
[24] Li N, Tan S, Wang Y, Deng J, Wang N, Zhu S, *et al*. *Akkermansia muciniphila* supplementation prevents cognitive impairment in sleep-deprived mice by modulating microglial engulfment of synapses. Gut Microbes. 2023; 15: 2252764. https://doi.org/10.1080/19490976.2023.2252764.
[25] Zhang N, Gao X, Li D, Xu L, Zhou G, Xu M, *et al*. Sleep deprivation-induced anxiety-like behaviors are associated with alterations in the gut microbiota and metabolites. Microbiology Spectrum. 2024; 12: e0143723. https://doi.org/10.1128/spectrum.01437-23.
[26] Yoon HS, Cho CH, Yun MS, Jang SJ, You HJ, Kim JH, *et al*. Akkermansia muciniphila secretes a glucagon-like peptide-1-inducing protein that improves glucose homeostasis and ameliorates metabolic disease in mice. Nature Microbiology. 2021; 6: 563–573. https://doi.org/10.1038/s41564-021-00880-5.
[27] Zheng PP, Zhang LN, Zhang J, Chang XM, Ding S, Xiao F, *et al*. Evaluating the Effects of Different Sleep Supplement Modes in Attenuating Metabolic Consequences of Night Shift Work Using Rat Model. Nature and Science of Sleep. 2020; 12: 1053–1065. https://doi.org/10.2147/NSS.S271318.
[28] Zhang M, Zhang M, Kou G, Li Y. The relationship between gut microbiota and inflammatory response, learning and memory in mice by sleep deprivation. Frontiers in Cellular and Infection Microbiology. 2023; 13: 1159771. https://doi.org/10.3389/fcimb.2023.1159771.
[29] Erben U, Loddenkemper C, Doerfel K, Spieckermann S, Haller D, Heimesaat MM, *et al*. A guide to histomorphological evaluation of intestinal inflammation in mouse models. International Journal of Clinical and Experimental Pathology. 2014; 7: 4557–4576.
[30] Tonet NS, da Silva Marçal DF, da Silva FN, Brunetta HS, Mori MADS, Dos Santos GJ, *et al*. Moderate chronic sleep perturbation impairs glucose and lipid homeostasis in rats. Sleep. 2024; 47: zsae118. https://doi.org/10.1093/sleep/zsae118.
[31] McHill AW, Hull JT, Klerman EB. Chronic Circadian Disruption and Sleep Restriction Influence Subjective Hunger, Appetite, and Food Preference. Nutrients. 2022; 14: 1800. https://doi.org/10.3390/nu14091800.
[32] Letchumanan G, Abdullah N, Marlini M, Baharom N, Lawley B, Omar MR, *et al*. Gut Microbiota Composition in Prediabetes and Newly Diagnosed Type 2 Diabetes: A Systematic Review of Observational Studies. Frontiers in Cellular and Infection Microbiology. 2022; 12: 943427. https://doi.org/10.3389/fcimb.2022.943427.
[33] Zhang X, Shen D, Fang Z, Jie Z, Qiu X, Zhang C, *et al*. Human gut microbiota changes reveal the progression of glucose intolerance. PloS One. 2013; 8: e71108. https://doi.org/10.1371/journal.pone.0071108.
[34] Zhou Q, Pang G, Zhang Z, Yuan H, Chen C, Zhang N, *et al*. As-

sociation Between Gut *Akkermansia* and Metabolic Syndrome is Dose-Dependent and Affected by Microbial Interactions: A Cross-Sectional Study. Diabetes, Metabolic Syndrome and Obesity: Targets and Therapy. 2021; 14: 2177–2188. https://doi.org/10.2147/DMSO.S311388.

[35] Michels N, Zouiouich S, Vanderbauwhede B, Vanacker J, Indave Ruiz BI, Huybrechts I. Human microbiome and metabolic health: An overview of systematic reviews. Obesity Reviews: an Official Journal of the International Association for the Study of Obesity. 2022; 23: e13409. https://doi.org/10.1111/obr.13409.

[36] Jin S, Lu Y, Zuo Y, Xu Q, Hao Y, Zuo H, *et al*. Akkermansia muciniphila ameliorates chronic stress-induced colorectal tumor growth by releasing outer membrane vesicles. Gut Microbes. 2025; 17: 2555618. https://doi.org/10.1080/19490976.2025.2555618.

[37] Khalili L, Park G, Nagpal R, Bhide P, Salazar G. The Impact of Akkermansia muciniphila on Mouse Models of Depression, Anxiety, and Stress: a Systematic Review and Meta-Analysis. Current Neuropharmacology. 2025; 23: 1423–1441. https://doi.org/10.2174/011570159x360149250225041829.

[38] Zheng LM, Li Y. Modifications in the Composition of the Gut Microbiota in Rats Induced by Chronic Sleep Deprivation: Potential Relation to Mental Disorders. Nature and Science of Sleep. 2024; 16: 1313–1325. https://doi.org/10.2147/NSS.S476691.

[39] Xiang X, Chen J, Zhu M, Gao H, Liu X, Wang Q. Multiomics Revealed the Multi-Dimensional Effects of Late Sleep on Gut Microbiota and Metabolites in Children in Northwest China. Nutrients. 2023; 15: 4315. https://doi.org/10.3390/nu15204315.

[40] Nollet M, Wisden W, Franks NP. Sleep deprivation and stress: a reciprocal relationship. Interface Focus. 2020; 10: 20190092. https://doi.org/10.1098/rsfs.2019.0092.

[41] Choshen-Hillel S, Ishqer A, Mahameed F, Reiter J, Gozal D, Gileles–Hillel A, *et al*. Acute and chronic sleep deprivation in residents: Cognition and stress biomarkers. Medical Education. 2021; 55: 174–184. https://doi.org/10.1111/medu.14296.

[42] Touitou Y, Reinberg A, Touitou D. Association between light at night, melatonin secretion, sleep deprivation, and the internal clock: Health impacts and mechanisms of circadian disruption. Life Sciences. 2017; 173: 94–106. https://doi.org/10.1016/j.lfs.2017.02.008.

[43] Szataniak I, Packi K. Melatonin as the Missing Link Between Sleep Deprivation and Immune Dysregulation: A Narrative Review. International Journal of Molecular Sciences. 2025; 26: 6731. https://doi.org/10.3390/ijms26146731.

[44] Yang H, Chen X, Yu X, Sun B, Tao J, Chen X. Sleep Deprivation and Subchronic Arsenite Exposure Synergistically Induced Skeletal Muscle Aging by Disrupting Melatonin and Cortisol Secretion in Mice. Toxics. 2025; 13: 97. https://doi.org/10.3390/toxics13020097.

[45] Wang X, Wang Z, Cao J, Dong Y, Chen Y. Gut microbiota-derived metabolites mediate the neuroprotective effect of melatonin in cognitive impairment induced by sleep deprivation. Microbiome. 2023; 11: 17. https://doi.org/10.1186/s40168-022-01452-3.

[46] Voigt RM, Forsyth CB, Green SJ, Engen PA, Keshavarzian A. Circadian Rhythm and the Gut Microbiome. International Review of Neurobiology. 2016; 161: 193–205. https://doi.org/10.1016/bs.irn.2016.07.002.

[47] Niu L, Zhang F, Xu X, Yang Y, Li S, Liu H, *et al*. Chronic sleep deprivation altered the expression of circadian clock genes and aggravated Alzheimer's disease neuropathology. Brain Pathology. 2022; 32: e13028. https://doi.org/10.1111/bpa.13028.

[48] Leone V, Gibbons S, Martinez K, Hutchison A, Huang E, Cham C, *et al*. Effects of Diurnal Variation of Gut Microbes and High-Fat Feeding on Host Circadian Clock Function and Metabolism. Cell Host &Amp; Microbe. 2015; 17: 681–689. https://doi.org/10.1016/j.chom.2015.03.006.

[49] S D V, T M V, Siddhu NSS. Impact of Food Intake and Sleep Disturbances on Gut Microbiota. Cureus. 2024; 16: e70846. https://doi.org/10.7759/cureus.70846.

[50] Lee J, Kang J, Kim Y, Lee S, Oh CM, Kim T. Integrated analysis of the microbiota-gut-brain axis in response to sleep deprivation and diet-induced obesity. Frontiers in Endocrinology. 2023; 14: 1117259. https://doi.org/10.3389/fendo.2023.1117259.

[51] Liang G, Zheng W, Dai Y, Li Y, Hu X, Zhang L, *et al*. Tibetan Tea Alleviates the Intestinal Dysfunction in Sleep-Deprived Mice through Regulating Oxidative Stress and Inflammation-Related Intestinal Metabolisms. Molecular Nutrition & Food Research. 2025; 69: e70098. https://doi.org/10.1002/mnfr.70098.

[52] Li G, Gao M, Zhang S, Dai T, Wang F, Geng J, *et al*. Sleep Deprivation Impairs Intestinal Mucosal Barrier by Activating Endoplasmic Reticulum Stress in Goblet Cells. The American Journal of Pathology. 2024; 194: 85–100. https://doi.org/10.1016/j.ajpath.2023.10.004.

[53] Wang Z, Zhou L, Zheng Y, Zhong X, Huang R, Sun W, *et al*. Nuclear receptor Nr1d1 links sleep deprivation to intestinal homeostasis via microbiota-derived taurine. Journal of Translational Medicine. 2025; 23: 1106. https://doi.org/10.1186/s12967-025-07089-8.

[54] Zhang HY, Shu YQ, Li Y, Hu YL, Wu ZH, Li ZP, *et al*. Metabolic disruption exacerbates intestinal damage during sleep deprivation by abolishing HIF1$\alpha$-mediated repair. Cell Reports. 2024; 43: 114915. https://doi.org/10.1016/j.celrep.2024.114915.

[55] Wang N, Li C, Gao X, Huo Y, Li Y, Cheng F, *et al*. Co-exposure to lead and high-fat diet aggravates systemic inflammation in mice by altering gut microbiota and the LPS/TLR4 pathway. Metallomics: Integrated Biometal Science. 2024; 16: mfae022. https://doi.org/10.1093/mtomcs/mfae022.

[56] Nyati KK, Masuda K, Zaman MMU, Dubey PK, Millrine D, Chalise JP, *et al*. TLR4-induced NF-κB and MAPK signaling regulate the IL-6 mRNA stabilizing protein Arid5a. Nucleic Acids Research. 2017; 45: 2687–2703. https://doi.org/10.1093/nar/gkx064.

[57] Everard A, Belzer C, Geurts L, Ouwerkerk JP, Druart C, Bindels LB, *et al*. Cross-talk between Akkermansia muciniphila and intestinal epithelium controls diet-induced obesity. Proceedings of the National Academy of Sciences of the United States of America. 2013; 110: 9066–9071. https://doi.org/10.1073/pnas.1219451110.

[58] Xie S, Li J, Lyu F, Xiong Q, Gu P, Chen Y, *et al*. Novel tripeptide RKH derived from *Akkermansia muciniphila* protects against lethal sepsis. Gut. 2023; 73: 78–91. https://doi.org/10.1136/gutjnl-2023-329996.

[59] Shen J, Wang S, Xia H, Han S, Wang Q, Wu Z, *et al*. *Akkermansia muciniphila* attenuated lipopolysaccharide-induced acute lung injury by modulating the gut microbiota and SCFAs in mice. Food & Function. 2023; 14: 10401–10417. https://doi.org/10.1039/d3fo04051h.

[60] Sonomoto K, Song R, Eriksson D, Hahn AM, Meng X, Lyu P, *et al*. High-fat-diet-associated intestinal microbiota exacerbates psoriasis-like inflammation by enhancing systemic $\gamma\delta$ T cell IL-17 production. Cell Reports. 2023; 42: 112713. https://doi.org/10.1016/j.celrep.2023.112713.

[61] Zhang L, Liu J, Jin T, Qin N, Ren X, Xia X. Live and pasteurized *Akkermansia muciniphila* attenuate hyperuricemia in mice through modulating uric acid metabolism, inflammation, and gut microbiota. Food & Function. 2022; 13: 12412–12425. https://doi.org/10.1039/d2fo02702j.

[62] Zhang Y, Liu R, Chen Y, Cao Z, Liu C, Bao R, *et al*. Akkermansia muciniphila supplementation in patients with overweight/obese type 2 diabetes: Efficacy depends on its baseline levels in the gut. Cell Metabolism. 2025; 37: 592–605.e6. https://doi.org/10.1016/j.cmet.2024.12.010.

[63] Lee HJ, Hong JK, Kim JK, Kim DH, Jang SW, Han SW, *et al*. Effects of Probiotic NVP-1704 on Mental Health and Sleep in Healthy Adults: An 8-Week Randomized, Double-Blind, Placebo-Controlled Trial. Nutrients. 2021; 13: 2660. https://doi.org/10.3390/nu13082660.

[64] Ho YT, Tsai YC, Kuo TBJ, Yang CCH. Effects of *Lactobacillus plantarum* PS128 on Depressive Symptoms and Sleep Quality in Self-Reported Insomniacs: A Randomized, Double-Blind, Placebo-Controlled Pilot Trial. Nutrients. 2021; 13: 2820. https://doi.org/10.3390/nu13082820.

[65] Rehman K, Akash MSH, Liaqat A, Kamal S, Qadir MI, Rasul A. Role of Interleukin-6 in Development of Insulin Resistance and Type 2 Diabetes Mellitus. Critical Reviews in Eukaryotic Gene Expression. 2017; 27: 229–236. https://doi.org/10.1615/CritRevEukaryotGeneExpr.2017019712.

[66] Akbari M, Hassan-Zadeh V. IL-6 signalling pathways and the development of type 2 diabetes. Inflammopharmacology. 2018; 26: 685–698. https://doi.org/10.1007/s10787-018-0458-0.